Journal of Computational Neuroscience (2019) 47:125–140
https://doi.org/10.1007/s10827-019-00730-8

Modeling cortical spreading depression induced by the hyperactivity of interneurons

Mathieu Desroches[1,2] · **Olivier Faugeras**[1,2] · **Martin Krupa**[1,2,3] · **Massimo Mantegazza**[2,4]

Received: 6 September 2018 / Revised: 14 March 2019 / Accepted: 5 September 2019 / Published online: 17 October 2019

Abstract

Cortical spreading depression (CSD) is a wave of transient intense neuronal firing leading to a long lasting depolarizing block of neuronal activity. It is a proposed pathological mechanism of migraine with aura. Some forms of migraine are associated with a genetic mutation of the $Na_{v1.1}$ channel, resulting in its gain of function and implying hyperexcitability of interneurons. This leads to the counterintuitive hypothesis that intense firing of interneurons can cause CSD ignition. To test this hypothesis in silico, we developed a computational model of an E-I pair (a pyramidal cell and an interneuron), in which the coupling between the cells in not just synaptic, but takes into account also the effects of the accumulation of extracellular potassium caused by the activity of the neurons and of the synapses. In the context of this model, we show that the intense firing of the interneuron can lead to CSD. We have investigated the effect of various biophysical parameters on the transition to CSD, including the levels of glutamate or GABA, frequency of the interneuron firing and the efficacy of the KCC2 co-transporter. The key element for CSD ignition in our model was the frequency of interneuron firing and the related accumulation of extracellular potassium, which induced a depolarizing block of the pyramidal cell. This constitutes a new mechanism of CSD ignition.

Keywords Cortical spreading depression · Migraine · Extracellular potassium · Interneuron hyperexcitability

1 Introduction

Cortical spreading depression (CSD) is a wave of transient intense neuronal firing leading to a long lasting depolarizing block of neuronal activity, which initiates focally and then slowly propagates in the cerebral cortex (Pietrobon and Moskowitz 2014). Long lasting spreading depolarizations of cortical circuits are involved in different pathophysiological conditions (Dreier 2011). Metabolically compromised injured brain tissue (in stroke, trauma and subarachnoid hemorrhage) generates anoxic spreading depolarizations that lead to cell death or long-lasting damage. In contrast, CSD generated in normoxic tissue does not cause neuronal death, is reversible and is a proposed pathological mechanism of migraine with aura (Lauritzen 1994; Pietrobon and Moskowitz 2014; Ferrari et al. 2015). In this condition, CSD causes transient neurological symptoms preceding the headache (the aura phase). It has been proposed that the CSD-dependent stimulation of trigeminal nociceptor nerve fibers innervating the blood vessels of the meninges causes the headache.

Some molecular/cellular mechanisms of CSD and migraine have been identified studying a rare form of genetic migraine with aura, characterized by hemiparesis during the attacks: familial hemiplegic migraine (FHM). FHM type 1 (FHM-1) is caused by gain of function mutations of the alpha1 subunit of the $Ca_V2.1$ P/Q type Ca^{2+} channel (*CACNA1A* gene) (Ophoff et al. 1996); FHM-2 is caused by loss-of-function mutations of the alpha2

Action Editor: Ken Miller

✉ Martin Krupa
martin.krupa@unice.fr

1 MathNeuro Team, Inria Sophia Antipolis Méditerranée, 06902, Sophia Antipolis Cedex, France

2 Université Côte d'Azur, 06108, Nice Cedex 2, France

3 JAD Laboratory, Université de Nice Sophia Antipolis, 06108, Nice Cedex 2, France

4 CNRS UMR7275, Institute of Molecular and Cellular Pharmacology (IPMC), LabEx ICST, 06560, Valbonne-Sophia Antipolis, France

subunit of the glial Na^+/K^+ pump (*ATP1A2* gene) (De Fusco et al. 2003). Facilitation of experimentally induced CSD has been reported in knock-in FHM-1 and FHM-2 mouse models (van den Maagdenberg et al. 2004; Leo et al. 2011). Moreover, it has been shown that FHM mutations in these mouse models cause increased glutamatergic transmission and extracellular glutamate accumulation (Tottene et al. 2009; Vecchia et al. 2014; Capuani et al. 2016), consistently with a similar overall mechanism.

FHM-3 is caused by mutations of the $Na_V1.1$ sodium channel (*SCN1A* gene) (Dichgans et al. 2005), and the pathological mechanism of these mutations is less well understood (Vecchia and Pietrobon 2012). $Na_V1.1$ is particularly important for generating GABAergic neurons' excitability (the neurons that classically have an inhibitory role in mature cortical circuits), and its mutations have been identified also in epileptic patients (Yu et al. 2006; Guerrini et al. 2014). Epileptogenic $Na_V1.1$ mutations cause loss-of-function of the channel with consequent decreased excitability of GABAergic neurons, reduced inhibition and hyperexcitability of cortical networks (Yu et al. 2006; Ogiwara et al. 2007; Han et al. 2012; Hedrich et al. 2014). Conversely, although initially loss of function has been reported also for FHM-3 $Na_V1.1$ mutations (Kahlig et al. 2008), more recent research provides evidence that these mutations cause instead a gain-of-function of the channel leading to hyperexcitability of GABAergic neurons in transfected cells in culture (Cestèle et al. 2008; Cestèle et al. 2013; Cestèle et al. 2013; Fan et al. 2016; Mantegazza and Cestele 2017). These results point to a different, counterintuitive mechanism in comparison to FHM-1 and FHM-2 mutations. In fact, it is not clear how increased activity of GABAergic neurons could trigger CSD, because it should reduce excitability of neuronal networks.

Three mechanisms (possibly acting in parallel) have been hypothesized for the ignition of CSD upon hyperexcitability of GABAergic interneurons (Cestèle et al. 2008; Cestèle et al. 2013; Cestèle et al. 2013; Mantegazza and Cestele 2017): 1) the extracellular potassium build-up generated by the potassium currents activated by the spiking of the interneurons, 2) the potassium build-up generated by the KCC2 co-transporter of the post synaptic pyramidal neurons, and 3) excitatory actions of GABAergic transmission. The first mechanism is expected during high frequency firing of the (inter)neurons. The second one has been reported in conditions of intense GABAergic synaptic transmission, because the function of KCC2 is to co-transport chloride and potassium for maintaining a low intracellular chloride concentration in the pyramidal cells, leading to an efflux of potassium (Viitanen et al. 2010; Doyon et al. 2011; Kaila et al. 2014). The third one can come into play when the homeostatic mechanisms that keep the intracellular chloride concentration low (in particular KCC2) reach their limits, leading to a transient partial dissipation of the chloride gradient and to depolarizing excitatory actions upon activation of the GABA-A receptor (Lillis et al. 2012). These mechanisms could increase the excitability of pyramidal neurons, possibly leading to CSD.

We present here a modeling study undertaken to test the hypothesis that CSD can be ignited by hyperactivation of interneurons and, more generally, to identify the mechanism of ignition in our model. We implemented a simple model of a pair of interconnected neurons, a pyramidal glutamatergic neuron (excitatory, E) and a GABAergic interneuron (inhibitory, I) (Fig. 1). We investigated the effect of different levels of excitability of the interneuron on the pyramidal neuron, considering the depolarizing block of the pyramidal neuron as the initiation of CSD. The interaction between the two cells consists of a GABAergic synapse from the interneuron onto the pyramidal cell, and a glutamatergic synapse from the pyramidal cell onto the interneuron. In addition we included a glutamatergic autapse (excitatory self coupling from the pyramidal cell to itself), in order to take into the account the role of the glutamatergic input on the pyramidal cell. We developed our model extending the one of Wei et al. (2014), who used a Hodgkin-Huxley type neuron model to study the neuronal dynamics underlying the generation of spikes, epileptic activity and CSD. The same authors subsequently used this model for investigating the role of cell volume in the transitions between these phenomena (Ullah et al. 2015). In our model the pyramidal cell is an adapted version of the neuron of Wei et al. (2014), whereas for the interneuron we have used the Wang-Buzsaki model (Wang and Buzsáki 1996). Our work was primarily inspired by the experimental evidence of the gain of function of GABA-ergic neurons in the context of FHM-3, but, more generally, the goal has been to explore the role of interneurons in the generation of CSD. Earlier modeling studies pertinent to FHM-3 (Dahlem et al. 2014) did not consider the role played by the interneurons.

Under physiological conditions interneurons do not show lasting high frequency firing. Our study refers to pathological conditions under which the interneurons maintain high frequency firing, possibly due to the dysfunction of ion channels, as in the case of FHM, or other causes, for example high level of $[K]_o$. Our findings show that CSD can be ignited in our model as a result of the intense firing of the interneuron, whereas in the absence of firing of the interneuron the pyramidal cell does not undergo CSD, and with moderate firing frequency of the interneuron the pyramidal neuron is inhibited. Our results indicate that the extracellular potassium build-up generated by the firing of the interneuron is the key factor for the initiation of CSD in our model.

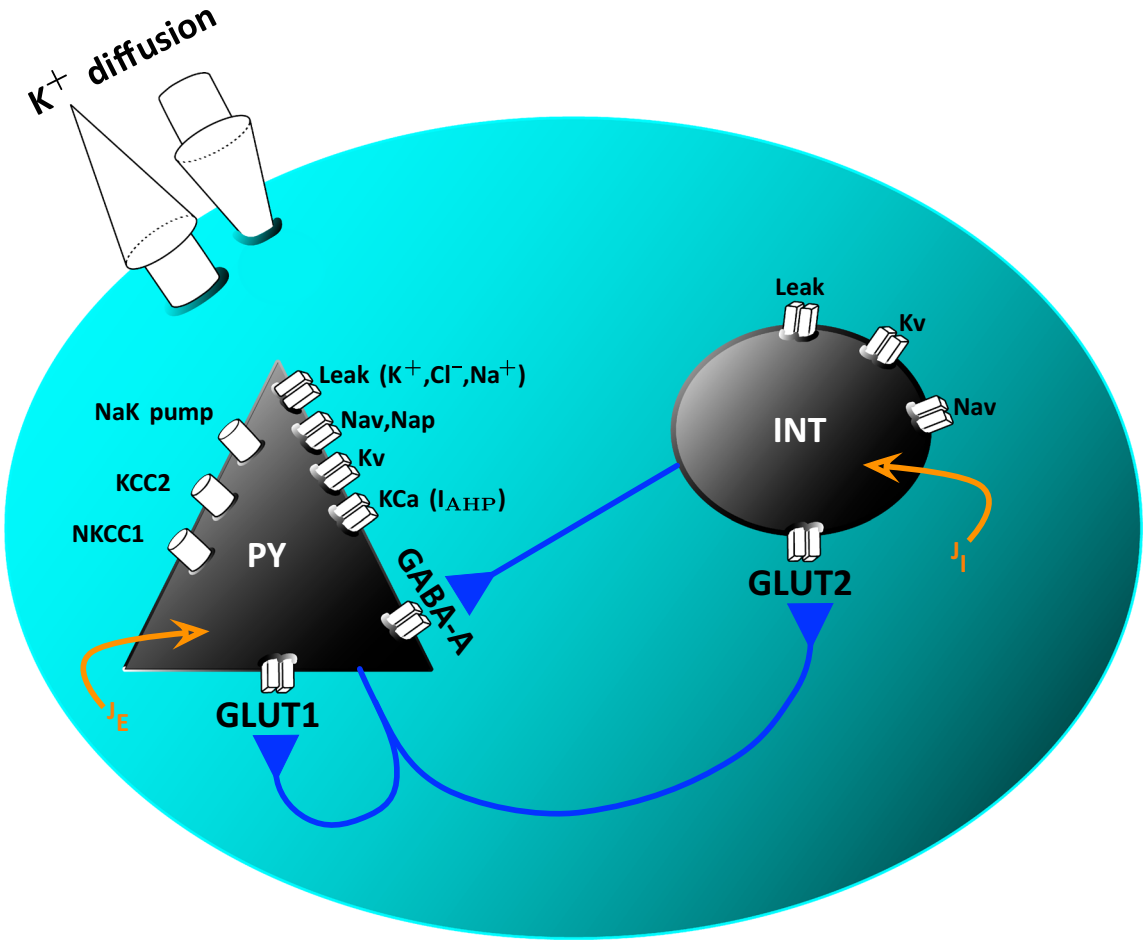

Fig. 1 Diagram of the model. The model implements a pair of interconnected neurons, a pyramidal glutamatergic neuron (excitatory, E) and a GABAergic interneuron (inhibitory, I). The interaction between the two cells consists of a GABAergic synapse (I_{GABA}) from the interneuron onto the pyramidal cell, a glutamatergic synapse from the pyramidal cell onto the interneuron (GLUT2), and a glutamatergic autapse (excitatory self coupling from the pyramidal cell to itself, GLUT1), in order to take into account the role of a glutamatergic input onto the pyramidal cell. It includes the action of the KCC2 and of the NKCC1 co-transporters in the pyramidal cell and the extracellular diffusion of potassium (for taking into account the diffusion in the extracellular space and spatial buffering by glia)

2 Methods

The model (Fig. 1) consists of an excitatory-inhibitory pair, more specifically a pyramidal cell and an interneuron, with a GABAergic synaptic connection from I to E, a glutamatergic synapse from E to I, and an autapse from E to itself. It includes the action of the KCC2 and of the NKCC1 co-transporters in the pyramidal cell and the extracellular diffusion of potassium (a simple diffusion equation for taking into account the diffusion in the extracellular space and spatial buffering by glia). Moreover, both the pyramidal cell and the GABAergic interneuron receive depolarizing drives (J_E and J_I, respectively, whose role is detailed below). Thus, the model is a microcircuit consisting of two interconnected neurons (glutamatergic and GABAergic), which can be used to mimic a cortical circuit and as a building block for implementing larger scale models. Our model is based on the model of Wei et al. (2014), see also Ullah et al. (2015).

2.1 Pyramidal cell

The spiking of the pyramidal cell is generated by a Traub-Miles (TM) model of a (hippocampal) pyramidal cell, given by the following system:

$$\begin{aligned} C\frac{dV}{dt} &= J_E - I_L - I_K - I_{Na} - I_{Nap} - I_{\mathrm{AHP}} \\ \frac{dn}{dt} &= \phi(\alpha_n(v)(1-n) - \beta_n(v)n) \\ \frac{dh}{dt} &= \phi(\alpha_h(v)(1-h) - \beta_h(v)h) \\ \frac{dCa}{dt} &= -\varepsilon g_{Ca} m_{\infty,1}(V - E_{Ca}) - \frac{Ca}{\tau_{Ca}}, \end{aligned} \tag{1}$$

with J_E representing the external drive (baseline current input), I_L the leak current, I_{Na} and I_K the usual spike generating sodium and potassium currents, and I_{Nap} the persistent slowly inactivating sodium current. Finally, I_{AHP} is a calcium activated potassium current, a so-called adaptation current. Thus, system Eq. (1) is obtained from a simplified version of the Traub-Miles model (Traub et al. 1991) by adding the adaptation current I_{AHP} and the persistent sodium current I_{Nap}. Most parameter values have been extracted from Börgers et al. (2005).

The currents appearing in the RHS of Eq. (1) were defined as follows: $I_L = g_L(v-E_L)$, $I_K = g_K n^4(v-E_K)$, $I_{Na} = g_{Na}m^3h(v-E_{Na})$, $I_{Nap} = g_p m^3(v-E_{Na})$ and $I_{\text{AHP}} = g_{\text{AHP}}\frac{Ca}{Ca+1}(V-E_K)$. The functions were defined as follows: $m_\infty(v) = \alpha_m(v)/(\alpha_m(v)+\beta_m(v))$, $\alpha_m(v) = 0.32(v+54)/(1-\exp^{-(v+54)/4})$, $\beta_m(v) = 0.28(v+27)/(\exp^{(v+27)/5}-1)$, $\alpha_h(v) = 0.128\exp^{-(v+50)/18}$, $\beta_h(v) = 4/(1+\exp^{-(v+27)/5})$, $\alpha_n(v) = 0.032(v+52)/(1-\exp^{-(v+52)/5})$ $m_{\infty,1} = 1/(1+\exp(-(V+25)/2.5))$ and $\beta_n(v) = 0.5\exp^{-(v+57)/40}$. The default parameter settings are as follows Börgers et al. (2005): $C = 1\mu$F, $g_{Na} = 100$mS/cm^2, $g_p = 1$mS/cm^2, $g_K = 80$mS/cm^2 and $\phi = 1$, $g_{\text{AHP}} = 1.5$mS/cm^2, $E_{Ca} = 120$mV, $g_{Ca} = 1$mS/cm^2, $\tau_{Ca} = 80$ms and $\varepsilon = 0.002(\text{ms}\mu\text{A})^{-1}\text{cm}^2$. We use different values of J_E, ranging from 3.4mA to 4mA.

The reversal potentials E_{Na}, E_K and E_{Cl} (the latter determining the I_{GABA} reversal potential) in computational models are typically set to be constant. In our model, they are slowly varying variables, as their variation is the cause of depolarizing block. The variable E_L is derived from E_K, E_{Cl} and E_{Na} (this will be discussed in detail below).

If a neuron maintains a homeostatic balance (ionic concentrations are quickly restored after a spike) then the assumption of constant reversal potentials made in the Hodgkin-Huxley model is justified. When the homeostatic balance is broken, for example in the case of CSD, it is necessary to include the dynamics of ionic concentrations. Other contexts where such modelling is needed include anoxic spreading depression (relevant to stroke) and epilepsy. Consequently there are a number of studies that use this type of modelling, including (Krishnan and Bazhenov 2011; Ullah et al. 2015; Wei et al. 2014; Dahlem et al. 2014; Chapuisat et al. 2008). In the construction of our model we follow closely the approach of Wei et al. (2014), see also Ullah et al. (2015). The originality of our work lies in the investigation of the effect of K^+ accumulation caused by intense interneuron firing on CSD ignition in the pyramidal cell.

2.2 Dynamic sodium, potassium and chloride concentrations

The evolution equations for the ionic concentrations, measured in mM=mol/l, are as follows:

$$\begin{aligned}
\frac{d[K]_o}{dt} &= \frac{1}{\tau}\big(\gamma\beta(I_K + I_{\text{AHP}} + I_{K,L} - 2I_{\text{pump}}) \\
&\qquad +\beta(I_{\text{KCC}} + I_{\text{NKCC}}) - I_{\text{sink}} + \gamma_i\beta I_{K,i}\big) \\
\frac{d[Na]_i}{dt} &= \frac{1}{\tau}(-\gamma(I_{Na}+I_{Nap}+I_{Na,L}+3I_{\text{pump}}) - I_{\text{NKCC}}) \\
\frac{d[Cl]_i}{dt} &= \frac{1}{\tau}\big(\gamma(I_{\text{GABA}} + I_{Cl,L}) - I_{\text{KCC}} - 2I_{\text{NKCC}}\big), \qquad (2)
\end{aligned}$$

where $[X]_i$ (resp. $[X]_o$) denotes the intracellular (resp. extracellular) concentration of the ionic species X. Here I_K, I_{AHP} and I_{Na} are as introduced above and $I_{K,L}$, $I_{Na,L}$ and $I_{Cl,L}$ are the individual leak currents. We will return to the leak current and its components later. We now describe the remaining terms and parameters contributing to system Eq. (2).

2.2.1 Co-transporters

I_{KCC} is the flux through the K–Cl co-transporter KCC2 (which extrudes potassium and chloride), as used in Wei et al. (2014), given by:

$$I_{\text{KCC}} = \rho_{\text{KCC}}\log\left(\frac{[K]_i[Cl]_i}{[K]_o[Cl]_o}\right),$$

and I_{NKCC} is the flux through the Na–K–Cl co-transporter NKCC, which transports sodium, potassium and chloride into the cells, given by:

$$\begin{aligned}
I_{\text{NKCC}} = \rho_{\text{NKCC}} f([K]_o)\Bigg(&\log\left(\frac{[K]_i[Cl]_i}{[K]_o[Cl]_o}\right) \\
&+\log\left(\frac{[Na]_i[Cl]_i}{[Na]_o[Cl]_o}\right)\Bigg),
\end{aligned}$$

with

$$f([K]_o) = \frac{1}{1+\exp(16-[K]_o)}.$$

The parameter settings are:

$$\rho_{\text{KCC}} = 0.3\text{mM/s} \quad \text{and} \quad \rho_{\text{NKCC}} = 0.1\text{mM/s}.$$

2.2.2 Sodium/potassium pump

The sodium potassium ATPase is the main mechanism restoring the ion concentrations to their steady state

values. The current through the pump is modelled as follows:

$$I_{\text{pump}} = \rho_{\text{pump}} \frac{1}{\gamma} \frac{1}{1+\exp\left((Na_{\text{sat}} - [Na]_i)/3\right)} \times \frac{1}{1+\exp(K_{\text{sat}} - [K]_o)},$$

where $\rho_{\text{pump}} = 0.25\text{mM/s}$, $Na_{\text{sat}} = 22\text{mM}$ and $K_{\text{sat}} = 3.5\text{mM}$.

2.2.3 Coupling currents from the interneuron

I_{GABA} is the chloride current generated by the GABA-A receptors of the inhibitory synapse; we will present it in more detail in the section on synaptic currents. $I_{K,i}$ is the potassium current of the interneuron, and it contributes to the dynamics of $[K]_o$, see Eq. (2), providing a form of coupling from the interneuron to the pyramidal cell, in addition to the GABAergic synapse.

2.2.4 The conversion factors β, γ, τ and γ_i

The parameter β is the ratio of the intracellular space of the pyramidal cell to the extracellular space and is set to $\beta = 4$, see Syková and Nicholson (2008).

The parameters γ and γ_i, whose units are M/(C·cm), are conversion factors from current density to the flux of ionic concentration, with γ corresponding to the pyramidal cell and γ_i to the interneuron. The parameter γ is given by $\gamma = S/(F \cdot \text{Vol})$, where S is the surface of the cell, Vol its volume, and F is the Faraday constant, with γ corresponding to the pyramidal cell, with

$$\text{Vol} = 1.4368 \cdot 10^{-9}\text{cm}^3, \quad S = 4\pi \left(\frac{3\text{Vol}}{4\pi}\right)^{2/3}. \tag{3}$$

The parameter γ_i plays a similar role for the potassium current of the interneuron, that is it converts this current into an ionic flux. In our simulations we used $\gamma_i = 0.65\gamma$ (Wei et al. 2014). The parameters γ/τ and γ_i/τ, where $\tau = 1000$, so that the units of the RHS of Eq. (2) are mM/ms.

2.2.5 Potassium sink

The expression modelling the diffusion of potassium in the extracellular space is

$$I_{\text{sink}} = \varepsilon_K([K]_o - K_{\text{bath}}), \tag{4}$$

with $\varepsilon_K = 0.4\text{s}^{-1}$ and $K_{\text{bath}} = 3.5\text{mM}$. This simple expression accounts for the removal of $[K]_o$. It models diffusion in the extracellular space but also (in an extremely simplified way) the spatial buffering performed by the glia. Note that, in comparison with Wei et al. (2014), we have kept this diffusion at a high level to make up for the absence of a glial current and a glial pump in our model.

2.2.6 Dynamics of the complementary ion concentrations

In addition we include the dynamics of $[K]_i$, given by

$$\frac{d[K]_i}{dt} = -\frac{1}{\tau}\left(\gamma\left(I_K + I_{AHP} + I_{K,L} - 2I_{\text{pump}}\right) + I_{KCC} + I_{NKCC}\right)$$

as well as require that

$$\frac{d}{dt}\left(\beta[Na]_i + [Na]_o\right) = \frac{d}{dt}\left(\beta[Cl]_i + [Cl]_o\right) = 0.$$

Hence $[Na]_o$ and $[Cl]_o$ also vary dynamically.

2.2.7 The reversal potentials

The reversal potentials correspond to the Nernst equilibrium, given by

$$E_K = \left(\frac{RT}{F}\right)\log\left(\frac{[K]_o}{[K]_i}\right)$$
$$E_{Na} = \left(\frac{RT}{F}\right)\log\left(\frac{[Na]_o}{[Na]_i}\right)$$
$$E_{Cl} = \left(\frac{RT}{F}\right)\log\left(\frac{[Cl]_o}{[Cl]_i}\right).$$

2.3 Leak current

The leak current I_L is the sum of a potassium leak current, a chloride leak current and a sodium leak current, that is:

$$I_L = g_{Na,L}(v - E_{Na}) + g_{K,L}(v - E_K) + g_{Cl,L}(v - E_{Cl}),$$

or, equivalently,

$$I_L = g_L(v - E_L), \tag{5}$$

with

$$g_L = (g_{Na,L} + g_{K,L} + g_{Cl,L}) \quad \text{and}$$
$$E_L = \frac{1}{g_L}(g_{Na,L}E_{Na} + g_{K,L}E_K + g_{Cl,L}E_{Cl}).$$

We have used in our simulations:

$$g_{Cl,L} = 0.015\text{mS/cm}^2, \quad g_{K,L} = 0.05\text{mS/cm}^2,$$
$$g_{Na,L} = 0.0015\text{mS/cm}^2.$$

Note that the setting of $g_{Na,L}$ is substantially lower than that from Wei et al. (2014).

2.4 Interneuron

The Wang-Buzsaki model of a fast spiking interneuron (PV+ basket cell) (Wang and Buzsáki 1996) is given by system Eq. (1) with

$$\begin{aligned}
\alpha_m &= 0.1(v+35.0)/(1.0-\exp(-(v+35.0)/10.0)),\\
\beta_m &= 4.0\exp(-(v+60.0)/18.0),\\
\alpha_h &= 0.07\exp(-(v+58.0)/20.0),\\
\beta_h &= 1.0/(1.0+\exp(-(v+28.0)/10.0)),\\
\alpha_n &= 0.01(v+34.0)/(1.0-\exp(-(v+34.0)/10.0)),\\
\beta_n &= 0.125\exp(-(v+44.0)/80.0),\\
m_\infty &= a_m/(a_m+b_m)
\end{aligned}$$

and the parameters: $g_{Na} = 35\text{mS/cm}^2$, $E_{Na} = 55\text{mV}$, $\phi = 5$, $g_L = 0.1\text{mS/cm}^2$, $E_L = -65\text{mV}$, $g_K = 9\text{mS/cm}^2$, and $E_K = -90\text{mV}$. (For the sake of simplicity we have chosen to use static (constant) reversal potentials in the interneuron model.) The external drive to the interneuron (baseline current input) is denoted by J_I and is varied between 0.6mA and 1.2 mA, corresponding to a firing frequency varying from approximately 40Hz to approximately 80Hz.

2.5 Synaptic currents

We modeled the synaptic coupling from the interneuron to the pyramidal cell, with the synaptic current:

$$I_{\text{GABA}} = g_{\text{GABA}} s(V - E_{Cl}). \tag{6}$$

For the dynamics of the synaptic variable, we used a simplified version of the model of Destexhe et al. (1994). The maximal GABA-A conductance, gGABA, was set to 0.5mS/cm^2, unless stated otherwise. The synaptic variable s is set to 1 following a spike of the interneuron and subsequently obeys the equation:

$$\frac{ds}{dt} = -\frac{1}{\tau_{\text{GABA}}} s,$$

with $\tau_{\text{GABA}} = 9$ ms. We have included an excitatory connection (GLUT1) from the pyramidal cell to itself (maximal conductance g_{GLUT1}) as well as an excitatory connection (GLUT2) from the pyramidal cell onto the interneuron (maximal conductance g_{GLUT2}), with associated currents $I_{\text{GLUT,E}} = g_{\text{GLUT1}}\tilde{s}_E(V_E - E_{\text{GLUT}})$ and $I_{\text{GLUT,I}} = g_{\text{GLUT2}}\tilde{s}_I(V_I - E_{\text{GLUT}})$, respectively, where E_{GLUT} will be kept at 0mV. The synaptic variables $\tilde{s}_E$ and $\tilde{s}_I$ follow a similar evolution equation as s, with a time constant $\tau_{\text{GLUT}} = 3$ms. The values of g_{GLUT1} and g_{GLUT2} will always be equal, hence we will denote both these maximal conductances by g_{GLUT}; they are set to 0.1mS/cm^2 unless stated otherwise.

2.6 Final voltage equation

The final form of the current balance in the pyramidal cell, with the addition of the synaptic current and the pump current (the balance of currents through KCC2 equals 0) is

$$C\frac{dV}{dt} = J_E - (I_L + I_K + I_{Na} + I_{Nap} + I_{\text{GABA}} + I_{\text{pump}} + I_{\text{GLUT}} + I_{\text{AHP}}).$$

The simulations were carried out on a MacBookPro laptop using the software package XPPAUT (Ermentrout 2002).

2.7 The meaning of the 'drive' parameters J_E and J_I.

The depolarizing drive parameters J_E and J_I should not be seen exclusively as external (glutamatergic) synaptic inputs, but as any features that can induce modifications of the activity of the neurons (basically any depolarizing currents). Little is known about the mechanisms that trigger pathological attacks in episodic paroxysmal disorders, in which patients are affected with symptoms sporadically. We implemented a "physiological network" and J_E and J_I can be seen as a mix of both physiological long range inputs and stimuli that drive the circuit into a pathological state. With these parameters it is possible to set the functional state of the different neurons in the microcircuit and study the effect on the response of the circuit.

3 Results

3.1 Interneuron firing can initiate spreading depression

As mentioned earlier, the main goal of this work is to develop a computational model of a cortical microcircuit for testing the hypothesis stating that intense firing of interneurons can initiate spreading depression. In our first simulation (Fig. 2) we chose initially a setting of the external excitatory drive to the pyramidal neuron (J_E) that gave tonic spiking of the pyramidal cell (between 10 and 15 spikes/s) in the absence of an active coupling with the interneuron (no GABAergic synaptic current and no influence of the K^+ efflux from the GABAergic neuron on the extracellular K^+ concentration: $g_{\text{GABA}} = 0\text{mS}$, $\gamma_i = 0\text{M/(C·cm)}$), and we investigated the modulatory effect of the GABAergic neurons firing at different frequencies. With an active coupling with the interneuron (both GABAergic synaptic current and K^+ efflux) and parameter settings (external excitatory drive to the interneuron J_I) leading to a moderate firing frequency (approximately 40Hz), the firing frequency of the pyramidal neuron was constantly reduced in the initial 15s of the simulation (Fig. 2a-b) and, for the rest

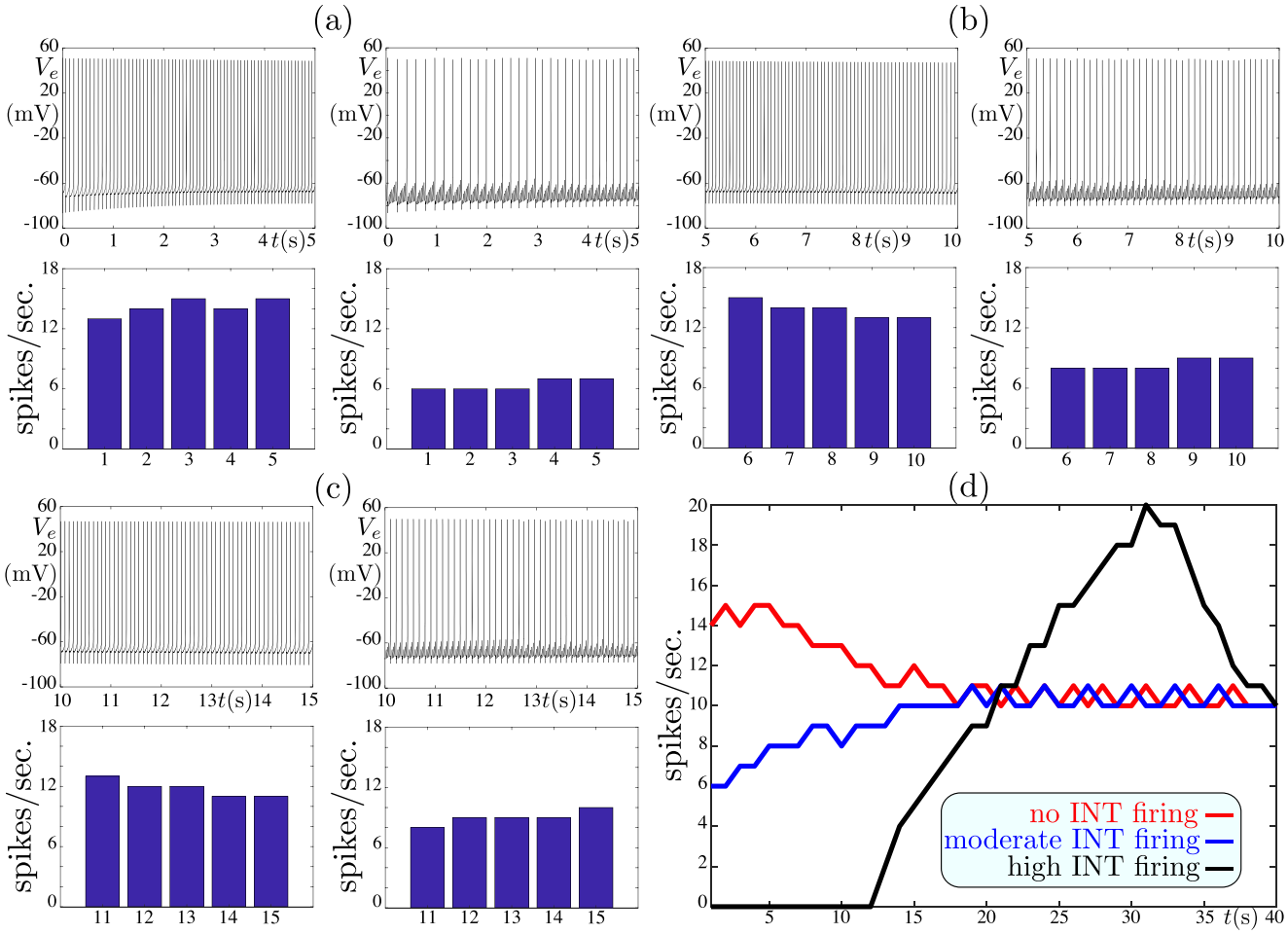

Fig. 2 Inhibitory effect of the interneuron spiking at moderate frequency. When the interneuron is set to fire at about 40Hz (J_I = 0.6mA), it exerts an inhibitory action on the firing of the pyramidal cell. When the coupling to the interneuron is active, the spiking of the pyramidal cell shows the largest reduction in the first 5 seconds, it remains slower than in the absence of inhibition during the first 15s (shown in panels **a**, **b**, **c**), and it does not exceed the firing frequency observed in the absence of inhibition even in later time windows (shown in panel **d**). When the firing rate of the interneuron is increased to approximately 70Hz the inhibitory effect is stronger at the outset, but it is followed by a period of hyperexcitability, where the pyramidal cell fires at a higher frequency then in the absence of the interneuron (shown in panel d). Panel **a** shows, in the top left corner the first 5s of the firing of the pyramidal cell (driven by $J_E = 4.5$mA) in the absence of the coupling to the interneuron ($g_{\mathrm{GABA}} = 0$mS and $\gamma_i = 0$M/(C·cm)). The bar graph immediately below shows the number of spikes in 1s time intervals. The right half of panel (**a**) shows the corresponding information when $\gamma_i = 0.65\gamma$ and $g_{\mathrm{GABA}} = 0.5$mS. Panel **b** shows the same information for the period 5-10 s. Panel **c** shows the same information for the period 10-15 s. The curves in panel (**d**) show how the firing frequency of the interneuron and the potassium efflux that it generates influence the spiking frequency of the pyramidal cell. These curves show the number of spikes per each of the first 40 seconds of the simulation for as a function of the activity of the interneuron. The blue curve corresponds to the absence the activity of the interneuron i.e. $g_{\mathrm{GABA}} = 0$mS and $\gamma_i = 0$M/(C·cm). The red curve corresponds to the case of moderate firing frequency of the interneuron ($J_I = 0.6$mA, i.e. approximately 40Hz, with $\gamma_i = 0.65\gamma$). The black curve corresponds to the case of elevated firing frequency of the interneuron ($J_I = 1.1$mA, i.e. approximately 70Hz)

of the simulation, it was approximately equal to the firing frequency of the pyramidal neuron observed in the absence of an active coupling with the interneuron: compare the blue and red curves in Fig. 2d.

Figure 2d shows the effect of varying the firing frequency of the interneuron. An increase of the firing frequency of the interneuron to about 60Hz gave rise to an initial inhibitory effect, which completely abolished the spiking of the pyramidal cell (Fig. 2d, black curve, time period 0-12s after the beginning of the simulation), followed by a period of hyperexcitability (between 20 and 40s after the beginning of the simulation), in which the frequency of the pyramidal cell became significantly higher (Fig. 2d black curve) than in the absence of the interneuron (see Fig. 2d blue curve). Thus, the increase of the firing frequency of the interneuron can lead in some time windows to increased excitability of the pyramidal cell. Notably, when the interneuron was set to spike at about 40Hz, the initial inhibitory effect that completely abolished the spiking of the pyramidal cell was not observed (Fig. 2d red curve).

In Fig. 3, we investigated the effect of a higher firing frequency of the interneuron. Strikingly, parameter settings leading to approximately 80Hz firing frequency for the interneuron ($J_I = 1.2$) initially abolished the spiking of the pyramidal cell, but subsequently, after a period of intense firing, induced a depolarizing block (Fig. 3) (b), which we consider in our model as the initiation of CSD. The onset of CSD was preceded by a significant rise of the extracellular potassium concentration ($[K]_o$, to about 12mM) at the threshold of CSD induction, and was concurrent with a large increase of $[K]_o$ up to about 35mM, which was accompanied by a slower increase of the intracellular chloride concentration ($[Cl]_i$, to about 15mM). In contrast, in the case of the tonic spiking of the pyramidal cell observed when the coupling with the interneuron was removed (Fig. 3a1), both $[K]_o$ and $[Cl]_i$ remained close to 5mM (Fig. 3b1). The baseline firing frequency of the pyramidal cell (6-15Hz) and of the interneuron (40-80Hz) in these simulations are well within physiological ranges. As highlighted above, the values of the parameters of the model are in the physiological range. The pathological state was set inducing a long lasting high frequency discharge of the interneuron by increasing its depolarizing drive (J_I). As highlighted above, this does not model only a long lasting increase of glutamatergic inputs onto the interneuron, but any stimulus that could induce overactivation of the interneuron and trigger a pathological state. For example, a mechanical stimulation (e.g. pinprick) can induce hyperexcitability and trigger CSD. A more speculative scenario would be a pathological gain of function of sodium currents of the interneuron (e.g. a large positive shift of the inactivation curve and/or an increase of the persistent component, as in Cestèle et al. (2013)) counteracted by the homeostatic increase of its K^+ currents; we could then imagine a hormonal inhibition of the K^+ currents (e.g. induced by a migraine trigger):

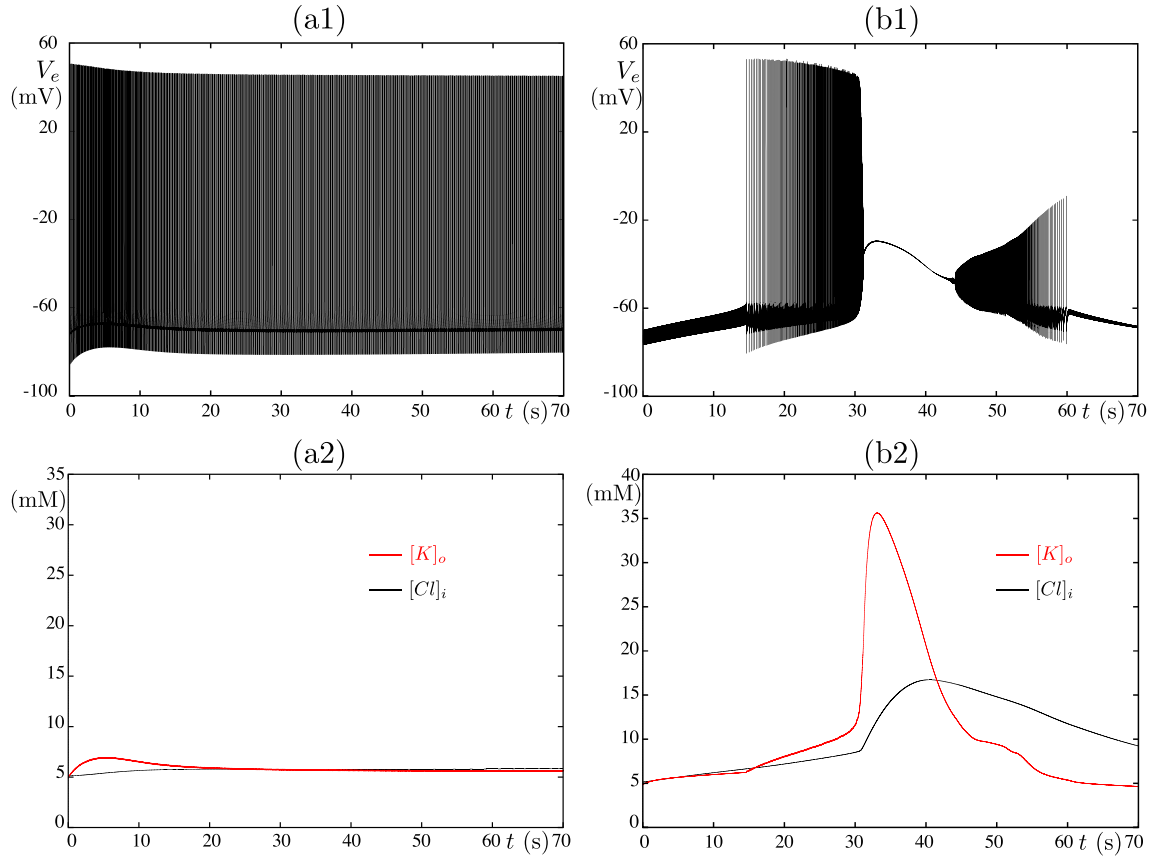

Fig. 3 The spiking of the pyramidal neuron can turn to spreading depression due to intense interneuron firing, which induces extracellular potassium build-up. Panel (a1) shows tonic spiking of the pyramidal cell induced by the excitatory drive $J_E = 4.5$mA when there is no coupling with the interneuron ($g_{GABA} = 0$mS and $\gamma_i = 0$M/(C·cm)): the same condition of the control in Fig. 2. Panel (a2) shows the evolution of the extracellular potassium concentration ($[K]_o$) and the intracellular chloride concentration ($[Cl]_i$) for the same simulation. The value of $[Cl]_i$ is almost constant throughout the simulation, close to 5 mM. Panel (b1) shows the depolarizing block of the pyramidal neuron (CSD) when $g_{GABA} = 0.5$mS and $\gamma_i = 0.65\gamma$ ($J_I = 1.2$mA, corresponding to the interneuron firing at approximately 80 Hz). Panel (b2) shows the evolution of $[K]_o$ and $[Cl]_i$ for the same simulation. Note a gradual increase in $[K]_o$ from about 10mM to about 12mM followed by sharp rise from 12mM to about 35mM, concurrent with the onset of spreading depression, and a slower increase of $[Cl]_i$ to about 15mM. The solutions in both simulations have the same initial condition

this would lead to a net inward current generated by the sodium channels of the interneuron also at resting potentials (modeled here as an increase of J_I), able to induce long-lasting hyperexcitability. Although speculative, this might be feasible in the framework of a paroxysmal episodic disorder (see also methods and discussion).

3.2 Factors that contribute to the onset of CSD

As shown above, an important factor determining the presence of CSD or hyperexcitability in our model is the baseline current input to the interneuron, J_I, which controls the firing frequency of the interneuron, thus the activation of its voltage dependent potassium currents that lead to K^+ efflux, as well as the strength of the GABAergic synaptic input onto the pyramidal neuron. The key pro-excitatory role of the extracellular potassium build-up generated by the potassium currents of the interneuron is evidenced in Fig. 3. This figure shows that the onset of CSD is accompanied by a rapid and substantial increase of $[K]_o$ (gradual increase from approximately 10mM to about 12mM followed by rapid increase from 12mM to about 34mM).

In another set of simulations we studied the effect of GABAergic and glutamatergic synaptic transmission on CSD onset. We set the parameters g_{GABA} and g_{GLUT} to $0mS$, exploring different combinations of such settings. Experimentally this would correspond to blocking the GABA and/or GLUT receptors. Figure 4 shows a sequence of simulations for increasing values of J_EmV (baseline excitatory drive of the pyramidal cell). For the lowest setting, $J_E = 3.9$mV, transition to CSD occurs only if GABA is blocked but GLUT is active ($g_{\mathrm{GABA}} = 0$mS and $g_{\mathrm{GLUT}} = 0.1$mS). This is illustrated in panels (a) and (b) of Fig. 4. Increasing excitatory drive (see panel (c)) to $J_E = 4.2$ is sufficient for CSD to occur with both GABA and GLUT blocked ($g_{\mathrm{GABA}} = g_{\mathrm{GLUT}} = 0$mS). However, if neither GABA nor GLUT are blocked (panel (d)), transition to CSD does not take place ($g_{\mathrm{GABA}} = 0.5$mS and $g_{\mathrm{GLUT}} = 0.1$mS). This is illustrated in panels (c) and (d) of Fig. 4. Finally, with $J_E = 4.5$mA, the transition to CSD occurs if neither GABA nor GLUT are blocked ($g_{\mathrm{GABA}} = 0.5$mS and $g_{\mathrm{GLUT}} = 0.1$mS), but it does not occur if GLUT is blocked ($g_{\mathrm{GLUT}} = 0$mS, $g_{\mathrm{GABA}} = 0.5$mS). This is illustrated in panels (e) and (f) of Fig. 4.

Overall, our findings show that both glutamate and potassium build-up contribute to the transition to spreading depression in our model, but GABAergic inhibition delays its onset. This suggests that the GABAergic transmission maintains its inhibitory character throughout the process of transition to CSD, and therefore delays it. This conclusion

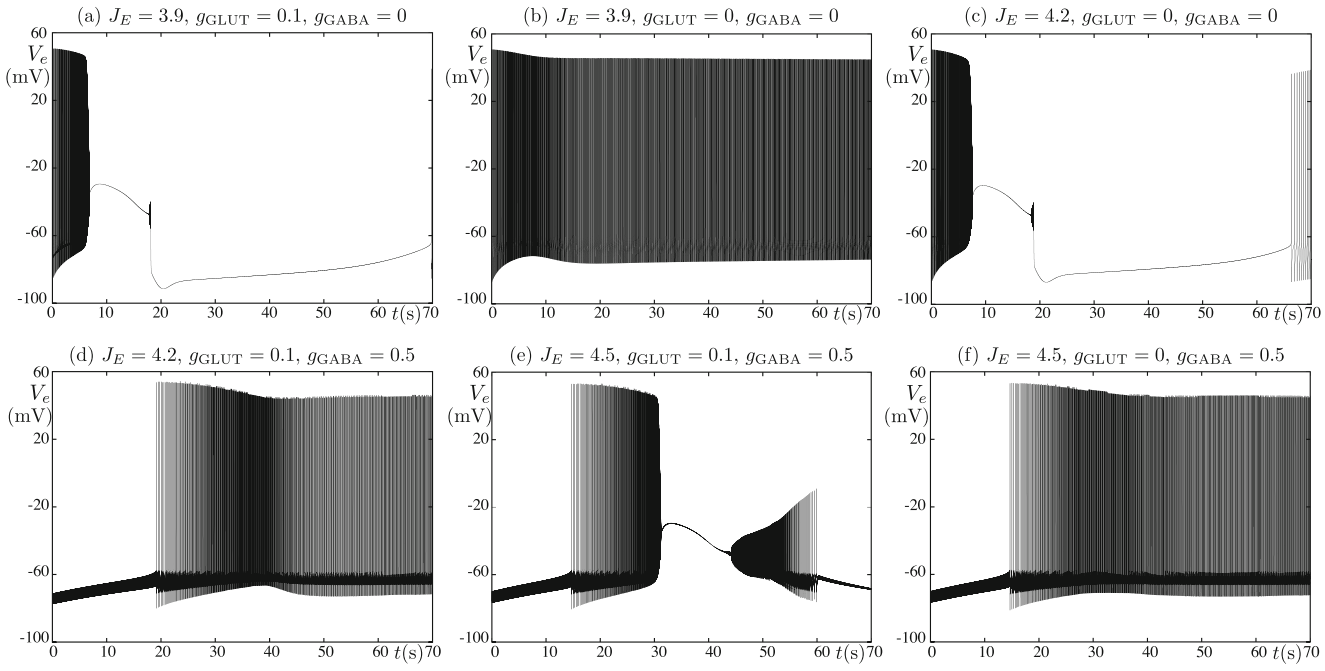

Fig. 4 GABAergic transmission delays CSD, whereas potassium build-up and glutamatergic transmission promote CSD. Panel **a** shows CSD for under a block of GABAergic transmission); the depolarizing block lasts approximately 13s. Panel **b** shows hyperexcitability but no CSD with a block of glutamatergic transmission. Panel **c** shows CSD with blocks of GABAergic and glutamatergic transmission; the depolarizing block lasts approximately 13s. Panel **d** shows hyperexcitability but no CSD with both GABAergic and glutamatergic transmission; the latency to spiking is approximately 18s. Panel **e** shows CSD with both GABAergic and glutamatergic transmission; the latency to spiking is approximately 14s. Panel **f** shows hyperexcitability but no CSD with no glutamatergic transmission but higher excitatory drive; the latency to spiking is approximately 14s. In all panels, we take $\gamma_i = 0.65\gamma$

is supported also by the slow increase of $[Cl]_i$ shown in Fig. 3b2, which is mainly observed after CSD onset. Conversely, the GLUT-mediated excitation speeds up CSD onset. Nonetheless, it is the activity of the interneuron that, through potassium build-up, leads to CSD. Figure 4c emphasizes the key role of extra-cellular potassium; it can trigger CSD even when synaptic transmission is blocked, whereas reactivation of both glutamatergic and GABAergic synaptic transmission blocked CSD induction (Fig. 4d). The simulation in which glutamatergic synaptic transmission is blocked but the depolarizing drive J_E is non-zero can be seen as an experimental condition in which glutamatergic synaptic transmission is blocked but a pathological stimulus that is not directly related to it is applied, for example a mechanical stimulation (pinprick). Another scenario could be the block of the local synaptic transmission by focal perfusion, without blocking long range inputs (this is experimentally possible in some brain areas, for example the hippocampus). However, in our simulation we aimed at testing the former condition. Figure 5 further shows the importance of K^+ efflux generated by the spiking of the interneuron in promoting the spiking of the pyramidal neuron and in eventually leading to CSD initiation. In fact, in a condition in which synaptic transmission was blocked and the pyramidal neuron fired regularly (same condition as in Fig. 4b), it was sufficient to increase the firing frequency of the interneuron to induce hyperexcitability of the pyramidal neuron and then its depolarizing block. It should be noted that the potassium from the interneuron is an effect that 'tips the scale', however a very significant contribution to the potassium efflux is given by the potassium current of the pyramidal cell. This is shown in Fig. 5 panels c1, c2 and

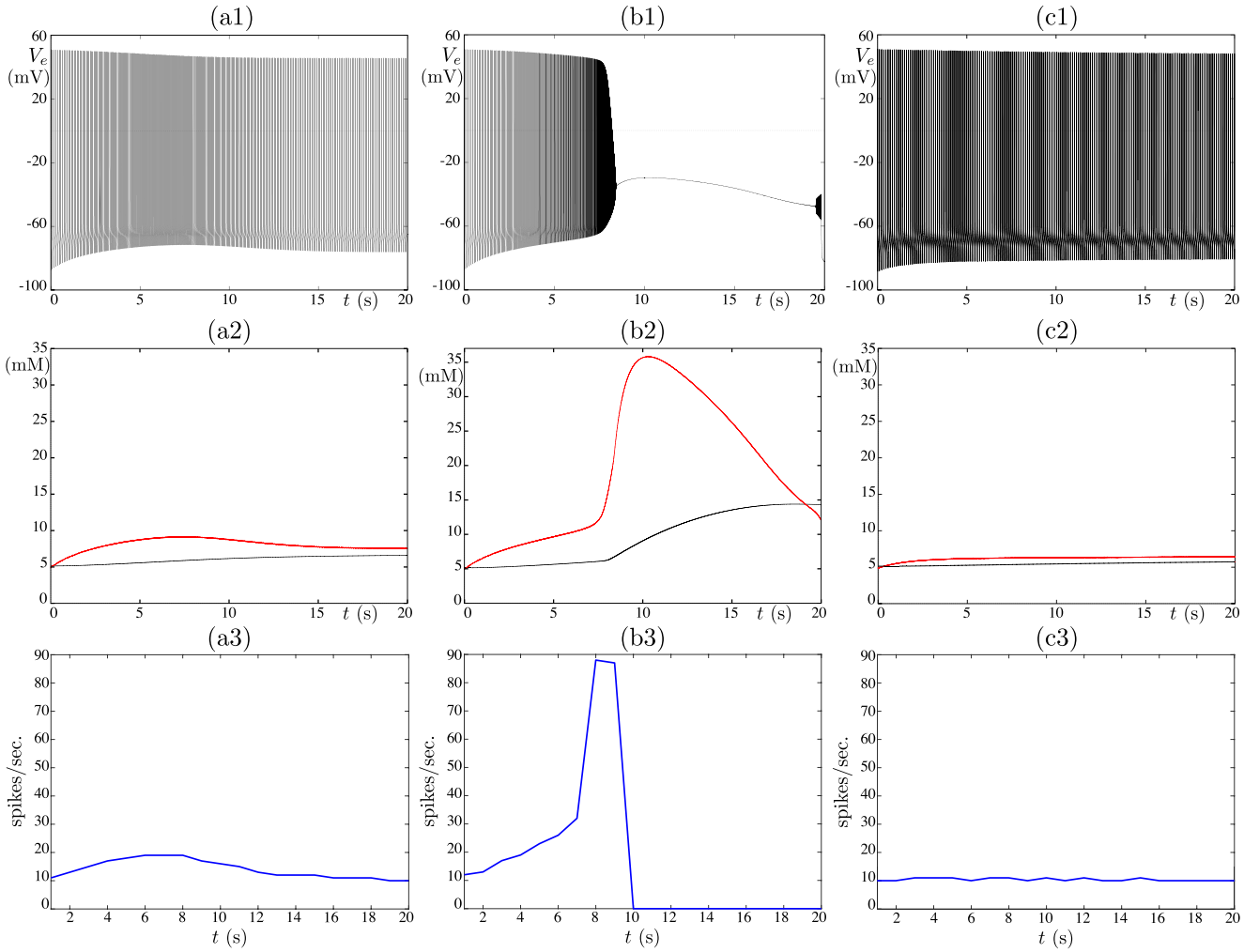

Fig. 5 Role of $[K]_o$ generated by the spiking of the interneuron inducing CSD. Starting from the parameter values corresponding to Fig. 4b in panels (a1,a2,a3), we increase the drive J_I to the interneuron from 1.2 to 1.5 in panels (b1,b2,b3) and this leads to CSD. Panels (c1,c2,c3) have the same settings as panels (b1,b2,b3) but with $\gamma = 0$ in the first equation of Eq. (2), which corresponds to neglecting the $[K]_o$ accumulation due to the firing of the pyramidal cell. Top rows corresponds to the PY time evolution; middle rows show the time profiles of $[K]_o$ (red) and of $[Cl]_i$ (black). Bottom rows show the number of spikes per second during the 20 second long simulations

c3, which represent a simulation with parameter values of Fig. 4b but without the contribution of the potassium current to $[K]_o$ (obtained by setting $\gamma = 0$ in the first equation of Eq. (2)).

We would like to point out a controversy concerning the role of glutamate in CSD initiation. Some studies show that the action of glutamate is necessary for CSD intiation, see Martins-Ferreira et al. (2000) for a review. Other studies show that, either blocking AMPA receptors has no effect on CSD, or that blocking NMDA receptors may reduce or stop CSD propagation but not CSD initiation, especially in the presence of high stimulation (Pietrobon and Moskowitz 2014). The results of our paper are consistent with Pietrobon and Moskowitz (2014), as we needed to increase the drive parameter J_E in order to trigger CSD in the absence of the glutamatergic input.

In addition to the classical fast inactivating transient sodium current, neurons show a slowly inactivating "persistent" current (I_{Nap}), which is important for shaping repetitive firing, generating rhythmicity and amplifying synaptic inputs (Stafstrom 2007). I_{Nap} has been found increased in different neurological diseases and it is implicated in some forms of spreading depolarizations (Mantegazza et al. 2010; Pietrobon and Moskowitz 2014). We tested the effect of an increase of I_{Nap} maximal conductance in our model. Figure 6 shows that increasing I_{Nap} leads to a decrease in the latency to spiking prior to CSD and a larger increase of $[K]_o$. I_{Nap} facilitates depolarizing block by increasing depolarization. Its presence leads to an increase in the activity of the sodium-potassium pump caused by the Na^+ influx, thereby increasing the pump current, which is hyperpolarizing and thus protects the cell against hyperexcitability and depolarizing block.

Finally, we have studied the effect of varying the activity of the KCC2 co-transporter. Our simulations show that increasing ρ_{KCC} does not prevent CSD but delays its onset

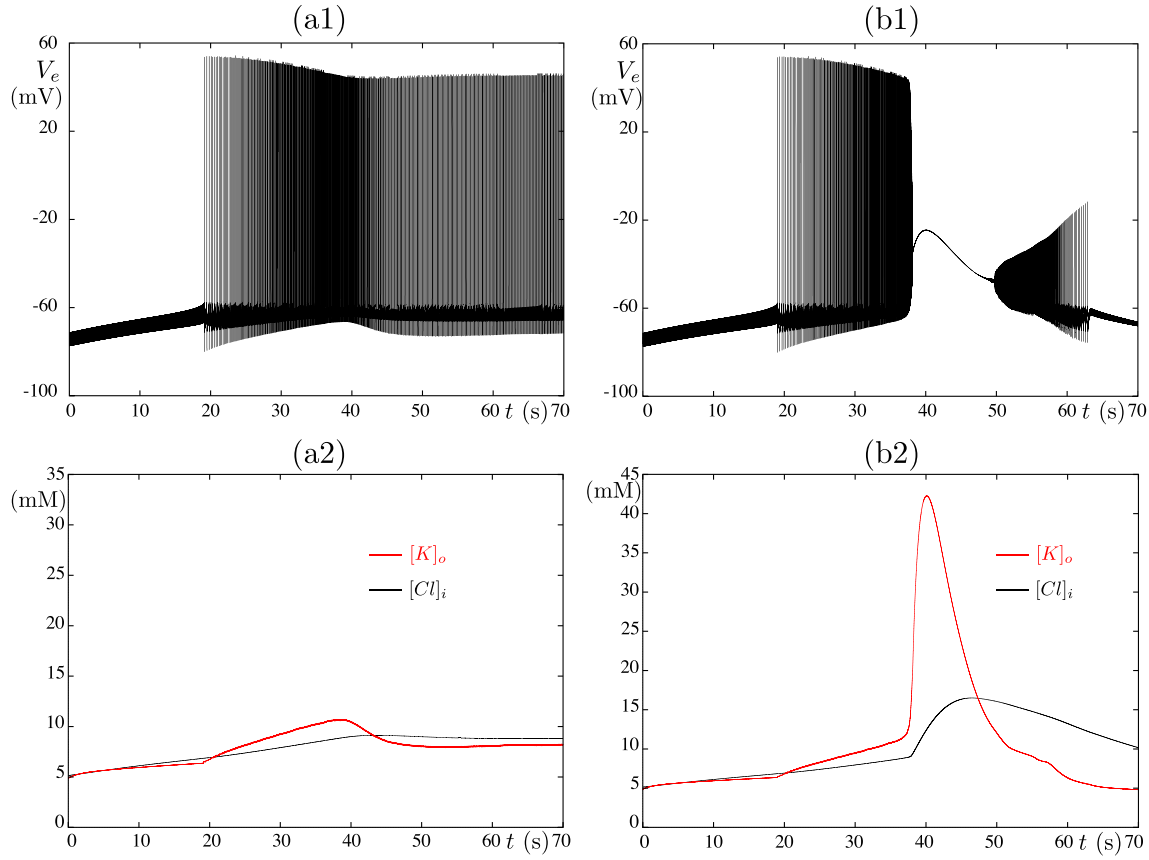

Fig. 6 The persistent sodium current (I_{Nap}) facilitates CSD ignition. Increasing I_{Nap} by setting $g_p = 3$mS has the effect of accelerating CSD. Panel (a1) shows hyperexcitability but no CSD for $g_{Nap} = 1$mS, $J_E = 4.2$mA, with $g_{\mathrm{GLUT1}} = g_{\mathrm{GLUT2}} = 0.1$mS, $\gamma_i = 0.65\gamma$ and $g_{\mathrm{GABA}} = 0.5$mS. Panel (a2) shows the corresponding potassium and chloride dynamics. Increasing g_p to 3mS (panels (b1-b2)) results in CSD. Note that latency to spiking in panels (a1) and (b1) is the same (about 19s). The length of the depolarizing block in panel (b1) is about 13s, approximately as in the case of Fig. 3b1 ($J_E = 4.5$mA, $g_p = 1$mS). Panel (b2) shows the corresponding potassium and chloride dynamics, with the $[K]_o$ peak higher than in the case of Fig. 3b2 ($J_E = 4.5$mA, $g_p = 1$mS), reaching 42mM, as opposed to 35mM. The latency to spiking in the simulation of Fig. 3 is approximately 14s and is lower than the approximately 19s in the present situation (the onset of spiking depends on the drive J_E as I_{Nap} activates close to the spiking threshold), but in the case of $g_p = 3$mS $[K]_o$ rises faster, leading to CSD

(see Fig. 7), consistent with an inhibitory role of KCC2 in this mechanism of CSD initiation.

3.3 Transitions to CSD seen as a dynamic bifurcation

The transition to CSD is characterized by rapid changes in the behavior of the variables. Figure 8 shows the time traces of the membrane potential of the pyramidal neuron (V_e) and of $[K]_o$ shortly before and during the transition to CSD. A remarkable feature is a very fast increase of $[K]_o$ in comparison to its earlier evolution. This can be explained as follows: previously to the onset of CSD there is a temporary balance (a transient steady state) between the effect of the potassium currents of the pyramidal cell and the interneuron (which leads to the increase of $[K]_o$), and the homeostatic mechanisms that decrease $[K]_o$ (e.g. the action of the sodium-potassium pump, the extracellular potassium diffusion/glial buffering). As the cell firing increases this balance is impaired (the steady state is no longer stable), which results in a rapid increase of $[K]_o$ as well as an average depolarization of V_e, levelling off at another transient steady state, which corresponds to CSD; see Fig. 8 panels a-b. Typically the concept of dynamic bifurcation is linked to the presence of multiple time scales, with slow variables seen as dynamic parameters and fast variables undergoing the bifurcations. Remarkably, the simulation in Fig. 8b suggests that $[K]_o$ evolves in this stage of the dynamics with comparable speed to the average of V_e, thus that the dynamic bifurcation involves at least these two variables. A similar situation was reported in Doyon et al. (2011).

4 Discussion

In this work we have developed and studied a model of a cortical microcircuit consisting of two coupled neurons, a pyramidal cell and a GABAergic interneuron, and diffusion of potassium (to take into the account diffusion in the extracellular space and glial spatial buffering). The coupling, in addition to the usual synaptic transmission, included the depolarizing effect of the potassium efflux

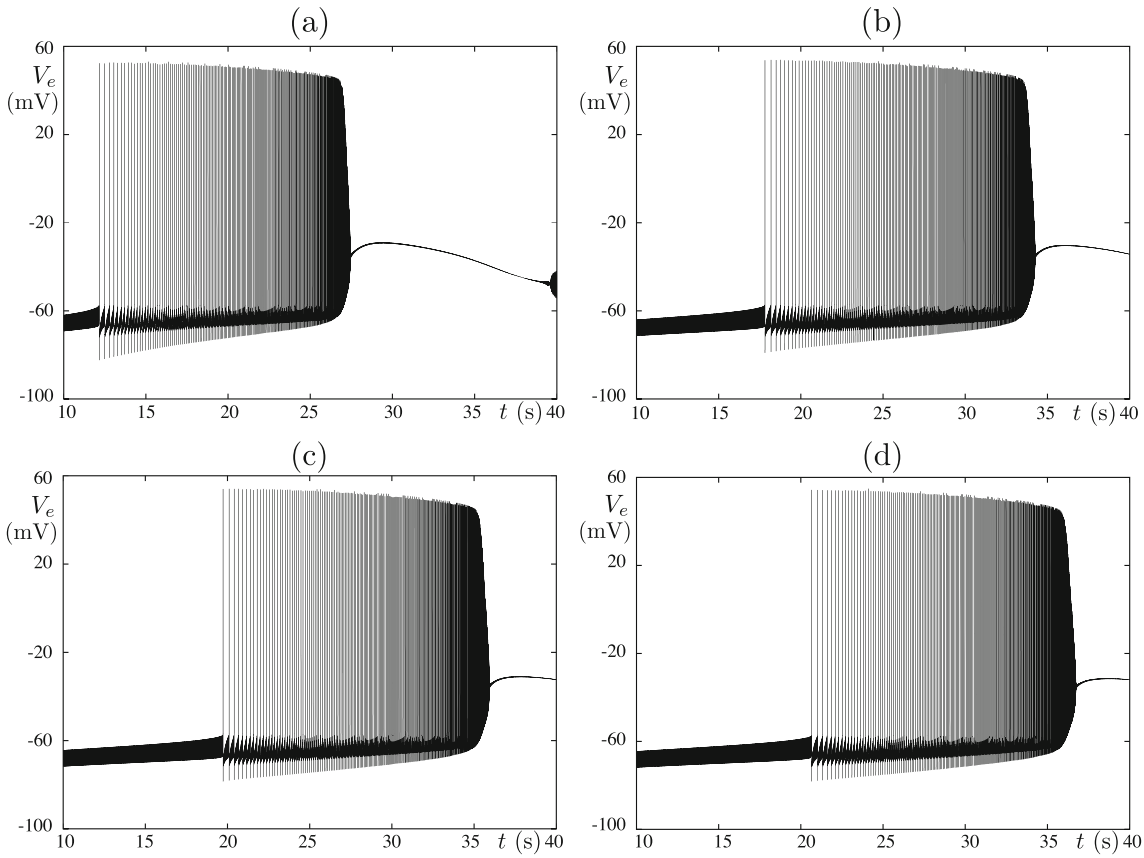

Fig. 7 Increasing ρ_{KCC} delays the onset of CSD. Transition to CSD for various values of ρ_{KCC} is shown, with $J_E = 4.5$mA, with $g_{GLUT1} = g_{GLUT2} = 0.1$mS, $\gamma_i = 0.65\gamma$ and $g_{GABA} = 0.5$mS. Panel **a** corresponds to $\rho_{KCC} = 0$mM/s, the latency to spiking is 12s. Panel **b** corresponds to $\rho_{KCC} = 1$mM/s, the latency to spiking is 17s. Panel **c** corresponds to $\rho_{KCC} = 2$mM/s, the latency to spiking is 19s. Panel **d** corresponds to $\rho_{KCC} = 3$mM/s, the latency to spiking is 21s. The simulation suggests that this effect is most pronounced for a window of intermediate ρ_{KCC} values and levels off for larger values

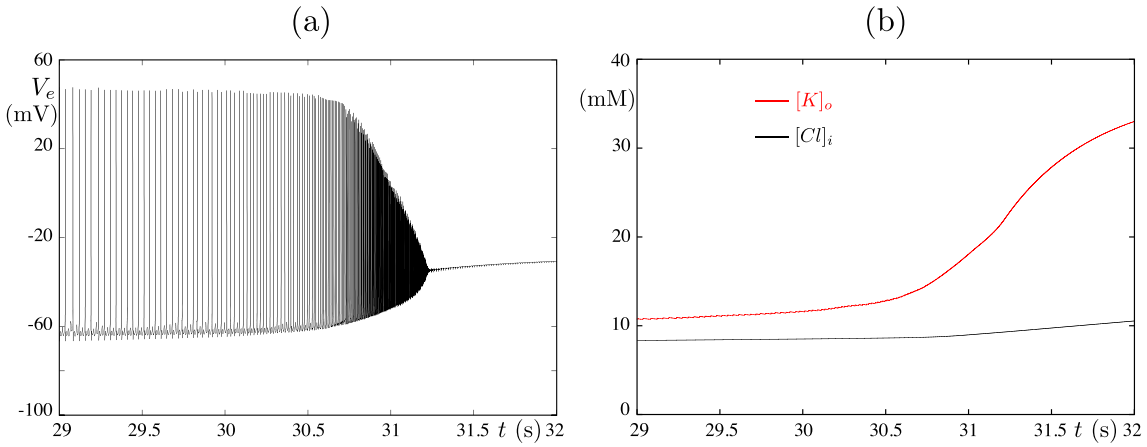

Fig. 8 Transitions to and from CSD as dynamic bifurcations. The figures represent zooms of Fig. 3a2 and b2 corresponding to different time intervals (J_E = 4mA, g_{GABA} = 0.25mS, $\gamma_i = 0.65\gamma$, $g_{\text{GLUT1}} = g_{\text{GLUT2}}$ = 0.1mS and J_I = 1.2mA). Panel **a** shows the time trace of the membrane potential of the pyramidal cell (V_e) directly before and during CSD. Note that the average of Ve is almost constant in the initial 2 seconds and grows quickly to a different level in the subsequent 2 seconds. Panel **b** shows a similar phenomenon for $[K]_o$. Panel **c** shows a transition that ends CSD, with the average of Ve sharply dropping. Panel **d** shows that $[K]_o$ changes uniformly during the transition ending CSD

due to the spiking of the interneuron and of the pyramidal cell. The pyramidal cell, besides the ion channels involved in the generation of action potentials, includes KCC2 and NKCC1 transporters implicated in intracellular chloride homeostasis. We used this model to test the hypothesis that hyperexcitability of GABAergic cortical neurons can lead to CSD, a possible pathological mechanism of migraine with aura (Lauritzen 1994; Pietrobon and Moskowitz 2014; Ferrari et al. 2015). This hypothesis has been proposed because migraine mutations of the $\text{Na}_V1.1$ sodium channel, which is particularly important for the excitability of GABAergic interneurons, can induce gain of function of the channel and hyperexcitability in transfected neurons (Cestèle et al. 2008; Cestèle et al. 2013; Cestèle et al. 2013; Mantegazza and Cestele 2017). However, this hypothesis has not been tested yet in a neuronal circuit and the detailed mechanism has not been addressed. In fact, GABAergic neurons are inhibitory in mature cortical circuits and their hyperexcitability should lead to inhibition of the circuits, instead of inducing CSD.

Our main finding is that CSD can be ignited by high frequency spiking of the interneuron in our model even if the GABAergic transmission maintains always inhibitory features. Long lasting high frequency spiking of the interneuron has been induced in our model by increasing J_I (which can be any physiological or pathological depolarizing drive; see results and methods). We could have implemented pathological modifications that are more directly related to clinical pathological mechanisms (e.g. effect of genetic mutations), but, even with these pathological dysfunction, patients experience attacks intermittently, and the mechanisms that trigger attacks are not clear. Thus we decided to set the microcircuit in a pathological state simply acting on J_I. Notably, long lasting modifications of neuronal excitability have been reported in paroxysmal episodic disorders, for example neurons in epileptic foci show long lasting hyperexcitability that begins minutes before the attack (seizure) (Truccolo et al. 2011). More generally, we have observed three possible effects of the interneuron on the firing of the pyramidal cell, depending on the interneuron's firing frequency. For low frequencies, the effect was inhibitory in the initial 5-10s and in the subsequent periods of the simulation the firing frequency was not increased. For higher frequencies, the activity of the interneuron increased the firing frequency of the pyramidal cell in a time window of the simulation. If the frequency of the interneuron was sufficiently high, a transition to CSD took place. Importantly, when the potassium build up caused by the interneuron firing was not taken into account, the interneuron had always an inhibitory effect, even when it fired at high frequency. Moreover, an increase of the firing frequency of the interneuron turned the regular firing of the pyramidal neuron into CSD even when GABAergic and glutamatergic synaptic transmission were blocked, condition in which the only interaction between the two cells was through modifications of the $[K]_o$. Hence, synaptic transmission can modulate positively induction of CSD but is not necessary for it. Notably, the spiking-induced efflux of K^+ from the interneuron and the pyramidal neuron were both necessary for CSD induction. This was shown by simulating the model with the contribution of the potassium current to the potassium efflux blocked, see Fig. 5c1, c2 and c3.

Interestingly, a larger persistent sodium current (I_{NaP}), similar to that observed in some neurologic conditions [23,

26], facilitated CSD induction and generated a stronger increase of the $[K]_o$ during the depolarizing block. This effect could facilitate the propagation of CSD in the cortical tissue. We have not tested this issue with our model, but it would be interesting to investigate it with larger models of cortical circuits. On the contrary, the activity of the KCC2 co-transporter inhibited CSD in our model, probably because its main role was to keep $[Cl]_i$ low, maintaining the inhibitory strength of the GABAergic synaptic transmission. Dynamic bifurcations, typical of slow-fast systems, are characterized by rapid changes of the fast variables. Although we are aware of the presence of multiple timescales in our system, time scale separation is not explicit. Our simulations suggest that $[K]_o$ and the average of the membrane potential evolve on the same time scale, at least during the transition to CSD. Proper identification of the underlying slow-fast structure and the type of bifurcation that occurs could lead to a method of predicting how close the system is to the transition to CSD and whether the transition will happen or not for the given parameter set. Partial and somewhat inconsistent bifurcation pictures of CSD models were obtained in Wei et al. (2014) and Zandt et al. (2015), which used systems that were similar, although not identical, to the one that we have used. In particular our main bifurcation parameter is the excitatory drive to the interneuron, which determines its firing frequency and that differs from both of these studies. Consequently, we feel that there is a need for an additional bifurcation study. Often a useful approach is to design a minimal system (a 'toy model') with similar dynamics but simple enough so that the bifurcation structure can be clearly identified. This will be the subject of future work.

Another follow-up of our study would be first to add more biological details to our model, for instance by considering dynamic changes in cell volume during CSD, and then to consider a network model, including, in addition to $[K]_o$ diffusion, also long distance excitatory projections onto both pyramidal cells and interneurons, and glial spatial buffering of potassium, which may play a role in the context of a realistic network. Interesting questions are the minimal number of hyperexcitable GABAergic interneurons that are necessary for igniting a propagating CSD, and if there are conditions (parameter settings) for which CSD would be ignited but does not propagate (remains localized). These issues are important because long lasting high frequency firing of large populations of interneurons is not a common phenomenon. This has been proposed as the mechanism of some types of focal seizures (Avoli and de Curtis 2011), but for CSD ignition and propagation the interneuron population probably has to be larger. Migraine attacks, as epileptic seizures, are characterized by acute and transient presentation of symptoms in individuals that otherwise appear normal; they can be triggered by emotional, dietary or physical stimuli (Pietrobon and Moskowitz 2014; Ferrari et al. 2015). Thus, a trigger stimulus could amplify a local event and induce large scale hyperexcitability of GABAergic interneurons leading to CSD induction in a local area and subsequent propagation in the cortical tissue. Interestingly, interneurons' excitability can be regulated by neuromodulators and hormones (Freund and Katona 2007).

Our work contributes to show that interneuron hyperexcitability can be the pathological mechanism of FHM-3, consistently with the hypothesis based on the study of the functional effect of FHM-3 $Na_V1.1$ mutations in transfected cells, and it poses a more general question about the role of interneurons in migraine with aura. Possibly, dysfunctions leading to GABAergic interneurons' hyperexcitability (not limited to $Na_V1.1$) could constitute a more general group of pathological mechanisms in migraine with aura, a condition probably caused by numerous different mechanisms, as suggested by the different mechanisms already identified in the rare FHM phenotype. Thus, our study suggests that hyperexcitability of interneuron populations could play a critical role in CSD ignition, even if they are not its sole cause. Understanding these mechanisms in detail could lead to pharmacological advances in the treatment of migraine.

Funding Information European Union projects DESIRE (grant n. EFP7-602531 to MM) and Investissements d'Avenir-Laboratory of Excellence "Ion Channels Science and Therapeutics" (grant LabEx ICST ANR-11-LABX-0015-01 to MM). ERC Advanced Grant Nervi 227747 (to OF).

Compliance with Ethical Standards

Conflict of interests The authors declare that they have no conflict of interest.

References

Avoli, M., & de Curtis, M. (2011). GABAErgic synchronization in the limbic system and its role in the generation of epileptiform activity. *Progress in Neurobiology*, *95*, 104–132.

Börgers, C., Epstein, S., Kopell, N. (2005). Background gamma rhythmicity and attention in cortical local circuits: a computational study. *Proceedings of the National Academy of Sciences of the United States of America*, *102*, 7002–7007.

Capuani, C., Melone, M., Tottene, A., Bragina, L., Crivellaro, G., Santello, M., Casari, G., Conti, F., Pietrobon, D. (2016). Defective glutamate and k^+ clearance by cortical astrocytes in familial hemiplegic migraine type 2. EMBO Mol Med e201505944.

Cestèle, S., Scalmani, P., Rusconi, R., Terragni, B., Franceschetti, S., Mantegazza, M. (2008). Self-limited hyperexcitability: functional effect of a familial hemiplegic migraine mutation of the Nav1. 1 (SCN1a) na^+ channel. *The Journal of Neuroscience*, *28*, 7273–7283.

Cestèle, S., Labate, A., Rusconi, R., Tarantino, P., Mumoli, L., Franceschetti, S., Annesi, G., Mantegazza, M., Gambardella, A. (2013). Divergent effects of the T1174S SCN1a mutation associated with seizures and hemiplegic migraine. *Epilepsia*, *54*, 927–935.

Cestèle, S., Schiavon, E., Rusconi, R., Franceschetti, S., Mantegazza, M. (2013). Nonfunctional $Na_{v1.1}$ familial hemiplegic migraine mutant transformed into gain of function by partial rescue of folding defects. *Proceedings of the National Academy of Sciences of the United States of America*, *110*, 17546–17551.

Chapuisat, G., Dronne, M.A., Grenier, E., Hommel, M., Gilquing, H., Boissel, J.P. (2008). A global phenomenological model of ischemic stroke with stress on spreading depressions. *Progress in Biophysics and Molecular Biology*, *97*, 4–27.

De Fusco, M., Marconi, R., Silvestri, L., Atorino, L., Rampoldi, L., Morgante, L., Ballabio, A., Aridon, P., Casari, G. (2003). Haploinsufficiency of ATP1a2 encoding the na^+/k^+ pump 2 subunit associated with familial hemiplegic migraine type 2. *Nature Genetics*, *33*, 192–196.

Dahlem, M.A., Schumacher, J., Hübel, N. (2014). Linking a genetic defect in migraine to spreading depression in a computational model. *PeerJ*, *2*, e379.

Destexhe, A., Mainen, Z.F., Sejnowski, T.J. (1994). An efficient method for computing synaptic conductances based on a kinetic model of receptor binding. *Neural Computation*, *6*, 14–18.

Dichgans, M., Freilinger, T., Eckstein, G., Babini, E., Lorenz-Depiereux, B., Biskup, S., Ferrari, M.D., Herzog, J., van den Maagdenberg, A.M., Pusch, M., Strom, T.M. (2005). Mutation in the neuronal voltage-gated sodium channel SCN1a in familial hemiplegic migraine. *Lancet*, *366*, 371–377.

Doyon, N., Prescott, S.A., Castonguay, A., Godin, A.G., Kröger, H., De Koninck, Y. (2011). Efficacy of synaptic inhibition depends on multiple, dynamically interacting mechanisms implicated in chloride homeostasis. *PLoS Computational Biology*, *7*, e1002149.

Dreier, J.P. (2011). The role of spreading depression, spreading depolarization and spreading ischemia in neurological disease. *Nature Medicine*, *17*, 439–447.

Ermentrout, B. (2002). Simulating, analyzing, and animating dynamical systems: a guide to XPPAUT for researchers and students. SIAM.

Fan, C. et al. (2016). Early-onset familial hemiplegic migraine due to a novel SCN1a mutation. *Cephalalgia*, *36*(13), 1238–1247.

Ferrari, M.D., Klever, R.R., Terwindt, G.M., Ayata, C., van den Maagdenberg, A.M. (2015). Migraine pathophysiology: lessons from mouse models and human genetics. *Lancet Neurology*, *14*, 65–80.

Freund, T.F., & Katona, I. (2007). Perisomatic inhibition. *Neuron*, *56*, 33–42.

Guerrini, R., Marini, C., Mantegazza, M. (2014). Genetic epilepsy syndromes without structural brain abnormalities: Clinical features and experimental models. *Neurotherapeutics*, *11*, 269–285.

Han, S., Tai, C., Westenbroek, R.E., Yu, F.H., Cheah, C.S., Potter, G.B., Rubenstein, J.L., Scheuer, T., de la Iglesia, H.O., Catterall, W.A. (2012). Autistic-like behaviour in $SCN1a^{+/-}$ mice and rescue by enhanced GABA-mediated neurotransmission. *Nat*, *489*, 385–390.

Hedrich, U.B., Liautard, C., Kirschenbaum, D., Pofahl, M., Lavigne, J., Liu, Y., Theiss, S., Slotta, J., Escayg, A., Dihne, M., Beck, H., Mantegazza, M., Lerche, H. (2014). Impaired action potential initiation in GABAergic interneurons causes hyperexcitable networks in an epileptic mouse model carrying a human Na(V)1.1 mutation. *Journal of Neuroscience*, *34*, 14874–14889.

Kahlig, K.M., Rhodes, T.M., Pusch, M., Freilinger, T., Pereira-Monteiro, J.M., Ferrari, M.D., van den Maagdenberg, A.M., Dichgans, M., George, A.L. Jr. (2008). Divergent sodium channel defects in familial hemiplegic migraine. *Proceedings of the National Academy of Sciences of the United States of America*, *105*, 9799–9804.

Kaila, K., Price, T.J., Payne, J.A., Puskarjov, M., Voipio, J. (2014). Cation-chloride cotransporters in neuronal development, plasticity and disease. *Nature Reviews Neuroscience*, *15*, 637–654.

Krishnan, G.P., & Bazhenov, M. (2011). Ionic dynamics mediate spontaneous termination of seizures and postictal depression state. *Journal of Neuroscience*, *31*(24), 8870–8882.

Lauritzen, M. (1994). Pathophysiology of the migraine aura. The spreading depression theory. *Brain: A Journal of Neurology*, *117*, 199–210.

Leo, L., Gherardini, L., Barone, V., De Fusco, M., Pietrobon, D., Pizzorusso, T., Casari, G. (2011). Increased susceptibility to cortical spreading depression in the mouse model of familial hemiplegic migraine type 2. *PLoS Genetics*, *7*, e1002129.

Lillis, K.P., Kramer, M.A., Mertz, J., Staley, K.J., White, J.A. (2012). Pyramidal cells accumulate chloride at seizure onset. *Neurobiology of Disease*, *47*, 358–366.

van den Maagdenberg, A.M., Pietrobon, D., Pizzorusso, T., Kaja, S., Broos, L.A., Cesetti, T., van de Ven, R.C., Tottene, A., van der, K.J., Plomp, J.J., Frants, R.R., Ferrari, M.D. (2004). A CACNA1a knockin migraine mouse model with increased susceptibility to cortical spreading depression. *Neuron*, *41*, 701–710.

Martins-Ferreira, H., Nedergaard, M., Nicholson, C. (2000). Perspectives on spreading depression. *Brain Research Reviews*, *32*(1), 215–234.

Mantegazza, M., & Cestele, S. (2017). Pathophysiological mechanisms of migraine and epilepsy: Similarities and differences. Neurosci Lett. https://doi.org/10.1016/j.neulet.2017.11.025.

Mantegazza, M., Curia, G., Biagini, G., Ragsdale, D.S., Avoli, M. (2010). Voltage-gated sodium channels as therapeutic targets in epilepsy and other neurological disorders. *Lancet Neurology*, *9*, 413–424.

Ogiwara, I., Miyamoto, H., Morita, N., Atapour, N., Mazaki, E., Inoue, I., Takeuchi, T., Itohara, S., Yanagawa, Y., Obata, K., Furuichi, T., Hensch, T.K., Yamakawa, K. (2007). Na(v)1.1 localizes to axons of parvalbumin-positive inhibitory interneurons: a circuit basis for epileptic seizures in mice carrying an SCN1a gene mutation. *Journal of Neuroscience*, *27*, 5903–5914.

Ophoff, R.A., Terwindt, G.M., Vergouwe, M.N., van Eijk, R., Oefner, P.J., Hoffman, S.M., Lamerdin, J.E., Mohrenweiser, H.W., Bulman, D.E., Ferrari, M., Haan, J., Lindhout, D., van Ommen, G.J., Hofker, M.H., Ferrari, M.D., Frants, R.R. (1996). Familial hemiplegic migraine and episodic ataxia type-2 are caused by mutations in the Ca2+ channel gene CACNL1a4. *Cell*, *87*, 543–552.

Pietrobon, D., & Moskowitz, M. (2014). Chaos and commotion in the wake of cortical spreading depression and spreading depolarizations. *Nature Reviews Neurology*, *15*, 379–392.

Stafstrom, C.E. (2007). Persistent sodium current and its role in epilepsy. *Epilepsy Curr*, *7*, 15–22.

Syková, E., & Nicholson, C. (2008). Diffusion in brain extracellular space. *Physiological Reviews*, *88*, 1277–1340.

Tottene, A., Conti, R., Fabbro, A., Vecchia, D., Shapovalova, M., Santello, M., van den Maagdenberg, A.M., Ferrari, M.D., Pietrobon, D. (2009). Enhanced excitatory transmission at cortical synapses as the basis for facilitated spreading depression in Ca(v)2.1 knockin migraine mice. *Neuron*, *61*, 762–773.

Traub, R.D., Wong, R.K., Miles, R., Michelson, H. (1991). A model of a CA3 hippocampal pyramidal neuron incorporating voltage-clamp data on intrinsic conductances. *Journal of Neurophysiology*, *66*, 635–650.

Truccolo, W., Donoghue, J.A., Hochberg, L.R., Eskandar, E.N., Madsen, J.R., Anderson, W.S., Brown, E.N., Halgren, E., Cash, S.S. (2011). Single-neuron dynamics in human focal epilepsy. *Nature Neuroscience*, *14*, 635–641.

Ullah, G., Wei, Y., Dahlem, M.A., Wechselberger, M., Schiff, S.J. (2015). The role of cell volume in the dynamics of seizure, spreading depression, and anoxic depolarization. *PLoS Computational Biology*, *11*, e1004414.

Vecchia, D., & Pietrobon, D. (2012). Migraine: a disorder of brain excitatory–inhibitory balance? *Trends in Neurosciences*, *35*, 507–520.

Vecchia, D., Tottene, A., van den Maagdenberg, A.M., Pietrobon, D. (2014). Mechanism underlying unaltered cortical inhibitory synaptic transmission in contrast with enhanced excitatory transmission in Ca2.1 knockin migraine mice. *Neurobiology of Disease*, *69*, 225–234.

Viitanen, T., Ruusuvuori, E., Kaila, K., Voipio, J. (2010). The K+-Cl cotransporter KCC2 promotes GABAergic excitation in the mature rat hippocampus. *Journal of Physiology*, *588*, 1527–1540.

Wei, Y., Ullah, G., Schiff, S.J. (2014). Unification of neuronal spikes, seizures, and spreading depression. *Journal of Neuroscience*, *34*, 11733–11743.

Wang, X.J., & Buzsáki, G. (1996). Gamma oscillation by synaptic inhibition in a hippocampal interneuronal network model. *Journal of Neuroscience*, *16*, 6402–6413.

Yu, F.H., Mantegazza, M., Westenbroek, R.E., Robbins, C.A., Kalume, F., Burton, K.A., Spain, W.J., McKnight, G.S., Scheuer, T., Catterall, W.A. (2006). Reduced sodium current in GABAergic interneurons in a mouse model of severe myoclonic epilepsy in infancy. *Nature Neuroscience*, *9*, 1142–1149.

Zandt, B.J., ten Haken, B., van Putten, M.J., Dahlem, M.A. (2015). How does spreading depression spread? Physiology and modeling. *Reviews in the Neurosciences*, *26*, 183–198.